

Helical Superconductors with Multiple Majorana Kramers Pairs in Rashba Bilayers

Qi-Sheng Xu,^{1,*} Zi-Ming Wang,^{1,*} Chui-Zhen Chen,² Lun-Hui Hu,^{3,†} Rui Wang,^{1,4,‡} and Dong-Hui Xu^{1,4,§}

¹Department of Physics and Chongqing Key Laboratory for Strongly Coupled Physics, Chongqing University, Chongqing 400044, China

²Institute for Advanced Study and School of Physical Science and Technology, Soochow University, Suzhou 215006, China

³Center for Correlated Matter and School of Physics, Zhejiang University, Hangzhou 310058, China

⁴Center of Quantum Materials and Devices, Chongqing University, Chongqing 400044, China

The momentum dependence of Rashba spin-orbit coupling (RSOC) is a key ingredient for engineering topological superconductors (TSCs), but research has largely focused on the linear-in-momentum form. This focus has restricted time-reversal invariant TSCs to helical p -wave states with only a single Majorana Kramers pair, whose existence is tied to the criterion of an odd number of Fermi surfaces (FSs). In this Letter, we demonstrate that a bilayer system with pure cubic RSOC and intrinsic odd-parity pairing on a single FS yields a rare 2D helical f -wave TSC. This state is characterized by a large mirror Chern number (MCN) of $\mathcal{N}_M = 3$ and hosts three Kramers pairs of Majorana edge modes. Remarkably, the interplay of linear and cubic RSOCs in this bilayer can generate a helical hybrid $p + f$ -wave TSC with an even larger MCN of $\mathcal{N}_M = 4$ from a normal state with two FSs, thereby circumventing the conventional odd-FS criterion. Our work establishes higher-order RSOC as a powerful design principle for realizing TSCs with multiple Majorana Kramers channels, fundamentally reshapes the helical hybrid for helical TSCs, and holds immediate relevance for tunable platforms like oxide heterostructures.

Spin-orbit coupling is the relativistic interaction between an electron's spin and its orbital motion. In crystals lacking inversion symmetry, this interaction manifests as Rashba spin-orbit coupling (RSOC), which lifts the spin degeneracy of electronic bands through momentum-dependent spin splitting [1]. RSOC is a cornerstone for realizing exotic quantum phenomena [2–6]. In superconductors, RSOC facilitates the admixture of spin-singlet and triplet Cooper pairs [7], significantly enhancing the upper critical field [7–9]. Crucially, the influence of RSOC is not limited to globally noncentrosymmetric materials; a hidden RSOC can emerge even in centrosymmetric structures, provided that local atomic environments break inversion symmetry [10–12]. This phenomenon, observed in systems such as bismuth-based cuprates [11] and heavy fermion superconductors [12], has significantly broadened the materials landscape for novel superconducting phases, particularly those characterized by odd-parity Cooper pairing [13].

A primary motivation for studying RSOC is its vital role in engineering topological superconductors (TSCs)—exotic states of matter that host Majorana quasiparticles. Seminal proposals have leveraged the spin-momentum locking of conventional, linear-in-momentum (\mathbf{k}) RSOC to generate TSCs. For instance, an s -wave superconductor proximitized to the surface of a topological insulator can realize an effective $p_x + ip_y$ state supporting Majorana zero modes in vortex cores [14]. By breaking time-reversal symmetry (TRS) with a magnetic field, two-dimensional (2D) systems with linear RSOC can host chiral p -wave TSCs [15–18]. Furthermore, linear RSOC is central to proposals for 2D helical TSCs that preserve TRS, whose existence is tied to the criterion of an odd number of Fermi surfaces (FSs) [19–21]. These states belong to symmetry class DIII and are characterized by a \mathbb{Z}_2 topological invariant, which protects a single Kramers pair of counterpropagating Majorana edge modes [22–25]. A crucial question, therefore, is how to transcend this binary framework to realize 2D TSCs with multiple Kramers pairs of Majorana channels, effectively transitioning from a \mathbb{Z}_2 to a \mathbb{Z} classification.

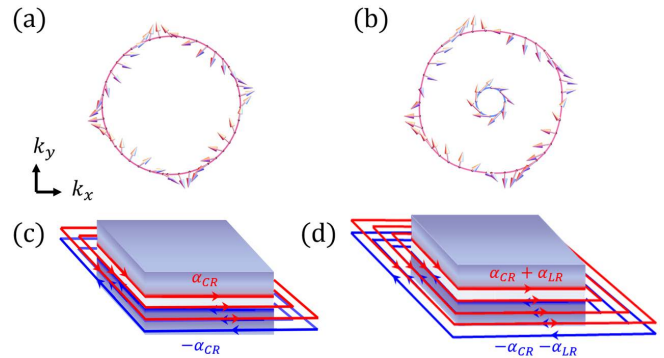


FIG. 1. Spin textures and their resulting helical Majorana channels. (a) Triple spin winding on a single FS due to cubic RSOC. (b) A combination of triple (outer FS) and single (inner FS) spin windings arising from the interplay of cubic and linear RSOC. (c, d) Helical Majorana edge modes in a mirror-symmetric bilayer induced by (c) cubic RSOC, resulting in three channels, and (d) coexisting linear and cubic RSOCs, which yields four channels.

A promising avenue involves exploring spin textures beyond the simple winding of the linear RSOC. Recently, significant attention has shifted towards a higher-order, cubic-in- \mathbf{k} RSOC [26–37], which can dominate when the linear term is suppressed by symmetry. This cubic RSOC is particularly relevant in oxide interfaces such as $\text{LaAlO}_3/\text{SrTiO}_3$ (LAO/STO), where its strength is electrically tunable [31, 38] and superconductivity is well established [39, 40]. The resulting spin textures are markedly different. Unlike linear RSOC, where the spin winds once around the FS [see spin texture of the inner FS in Fig. 1(b)], cubic RSOC generates a complex, triple-winding spin texture: as an electron encircles the FS, its spin rotates three times [Fig. 1(a)]. While prior work has explored proximity-induced, TRS-breaking TSCs [41–43], the potential for a TRS-invariant TSC driven by an intrinsic pairing instability in a cubic RSOC system—and the consequent realization of multiple Majorana Kramers pairs arising from its unique

triple-winding spin texture—remain key open questions.

In this Letter, we provide an affirmative answer and establish a direct mechanism for realizing novel TRS invariant helical TSCs that host multiple Kramers pairs of Majorana channels. We study an interacting bilayer model with local inversion symmetry breaking—a canonical platform for hidden RSOC. We find that the triple-winding spin texture inherent to cubic RSOC, combined with an odd-parity pairing instability on a single FS, leads to a TSC protected by mirror symmetry. The bulk topology is characterized by a large mirror Chern number (MCN), $\mathcal{N}_M = 3$, guaranteeing three Kramers pairs of Majorana edge modes [Fig. 1(c)]. Furthermore, we show that the coexistence of linear and cubic RSOCs can generate a helical hybrid $p + f$ -wave TSC characterized by $\mathcal{N}_M = 4$, hosting four Kramers pairs of Majorana edge modes [Fig. 1(d)]. Crucially, this state emerges from a normal state with two FSs, thereby circumventing the established odd-FS criterion for helical TSCs [19–21].

Model.—We consider a minimal model for locally noncentrosymmetric structures, realized by a 2D bilayer system possessing D_{4h} point group symmetry. While the system as a whole possesses global inversion symmetry, this symmetry is broken locally within the individual layers. This local asymmetry induces a hidden spin polarization [10–12], which manifests as a staggered RSOC in the bilayer geometry, as depicted in Figs. 1(c) and 1(d). The low-energy normal-state Hamiltonian describing this system is

$$\mathcal{H}_N(\mathbf{k}) = \epsilon_0(\mathbf{k})\tau_0 \otimes s_0 + \tau_z \otimes [\mathbf{g}(\mathbf{k}) \cdot \mathbf{s}] + \varepsilon\tau_x \otimes s_0, \quad (1)$$

where the Pauli matrices $\tau_{x,y,z}$ and $s_{x,y,z}$ act on the layer (lower (l), upper (u)) and spin (\uparrow, \downarrow) degrees of freedom, respectively, and τ_0 and s_0 are the corresponding 2×2 identity matrices. The first term, $\epsilon_0(\mathbf{k}) = \beta_0 k^4 + \beta_1 k^2$, describes the intralayer kinetic energy, where the quartic term can account for non-parabolic band effects. The second term represents the staggered RSOC, where τ_z ensures the RSOC has opposite signs in the two layers. The RSOC vector $\mathbf{g}(\mathbf{k}) = \mathbf{g}_{LR}(\mathbf{k}) + \mathbf{g}_{CR}(\mathbf{k})$ includes terms consistent with D_{4h} symmetry, which are linear and cubic in momentum \mathbf{k} : $\mathbf{g}_{LR}(\mathbf{k}) = \alpha_{LR}(-k_y, k_x, 0)$ and $\mathbf{g}_{CR}(\mathbf{k}) = \alpha_{CR}[-k_y(3k_x^2 - k_y^2), k_x(3k_y^2 - k_x^2), 0]$. The third term, with strength ε , is the momentum-independent interlayer tunneling, which opens a hybridization gap (HG) of 2ε around the Γ point [Fig. 2(a)]. The normal Hamiltonian, $\mathcal{H}_N(\mathbf{k})$, preserves several key symmetries: TRS represented by the antiunitary operator $\mathcal{T} = -is_y\mathcal{K}$ (where \mathcal{K} is the complex conjugate), inversion symmetry $\mathcal{I} = \tau_x$, fourfold rotational symmetry $\mathcal{R}_{4z} = i\tau_x e^{i\frac{\pi}{2} s_z}$ and mirror symmetry $\mathcal{M}_z = i\tau_x s_z$.

To investigate superconductivity, we introduce a phenomenological short-range density-density interaction, which has proven effective for studying competing pairing instabilities in various multi-orbital and multilayer systems [19, 23, 44]. The interaction Hamiltonian in real space is

$$\mathcal{H}_{\text{int}}(\mathbf{r}) = -U[n_l^2(\mathbf{r}) + n_u^2(\mathbf{r})] - 2Vn_l(\mathbf{r})n_u(\mathbf{r}), \quad (2)$$

where $n_\tau(\mathbf{r}) = \sum_s c_{\tau,s}^\dagger(\mathbf{r})c_{\tau,s}(\mathbf{r})$ is the local electron density operator in the lower ($\tau = l$) and upper ($\tau = u$) layers. The

parameters U and V represent the effective strengths of the intra-layer and inter-layer interactions, respectively; positive values correspond to attractive interactions. We then solve $\mathcal{H}_N + \mathcal{H}_{\text{int}}$ using the standard mean-field approximation. The interaction term is decoupled in the particle-particle (Cooper) channel, leading to momentum-independent pairing potentials whose symmetries are constrained D_{4h} . To formalize this, we introduce an eight-component Nambu spinor, defined as $\psi_{\mathbf{k}}^\dagger = (c_{l\mathbf{k},\uparrow}^\dagger, c_{l\mathbf{k},\downarrow}^\dagger, c_{u\mathbf{k},\uparrow}^\dagger, c_{u\mathbf{k},\downarrow}^\dagger, c_{l-\mathbf{k},\uparrow}, c_{l-\mathbf{k},\downarrow}, c_{u-\mathbf{k},\uparrow}, c_{u-\mathbf{k},\downarrow})$. The Bogoliubov-de Gennes (BdG) Hamiltonian takes the block form

$$\mathcal{H}_{\text{BdG}}(\mathbf{k}) = \begin{pmatrix} \mathcal{H}_N(\mathbf{k}) - \mu & \Delta(\mathbf{k}) \\ \Delta^\dagger(\mathbf{k}) & -\mathcal{H}_N^*(-\mathbf{k}) + \mu \end{pmatrix}, \quad (3)$$

where μ is the chemical potential, and $\Delta(\mathbf{k})$ is the 4×4 pairing potential matrix in the layer-spin space. The dominant pairing symmetries derived from the intralayer (U) and interlayer (V) interactions are summarized in Table I. The even-parity channel, transforming as the A_{1g} irrep, is a spin-singlet state. It contains two components: an intralayer pairing $\Delta_{1a} = \Delta_0(c_{l,\uparrow}c_{l,\downarrow} + c_{u,\uparrow}c_{u,\downarrow})$ and an interlayer pairing $\Delta_{1b} = \Delta_0(c_{l,\uparrow}c_{u,\downarrow} - c_{l,\downarrow}c_{u,\uparrow})$. Here, Δ_0 is the strength of the pairing potential. Because they share the same symmetry, these two components can mix. The remaining channels are all odd-parity and correspond to spin-triplet states. The Δ_2 (A_{1u}) and Δ_3 (A_{2u}) channels represent interlayer and intralayer pairings, respectively. $\Delta_{4x} = i\Delta_0(c_{l,\uparrow}c_{u,\uparrow} + c_{l,\downarrow}c_{u,\downarrow})$ and $\Delta_{4y} = \Delta_0(c_{l,\uparrow}c_{u,\uparrow} - c_{l,\downarrow}c_{u,\downarrow})$ belong to the 2D E_u irrep and describes an interlayer equal-spin pairing state.

Linearized gap equations and phase diagram.—For the subsequent analysis, we focus on the physics driven by the higher-order RSOC term. Therefore, we initially simplify the model by setting the linear Rashba coefficient to zero ($\alpha_{LR} = 0$), isolating the effects of the cubic RSOC. In the weak-coupling limit, we can determine the superconducting critical temperature T_c by solving the linearized gap equation, which can be expressed using the pairing susceptibility. The pairing susceptibility χ for a given pairing symmetry is calculated from the particle-particle correlation function

$$\begin{aligned} \chi_i &\equiv -\frac{1}{\beta_c} \sum_{\omega_n, \mathbf{k}} \text{Tr} \left[\Gamma_i^\dagger \mathcal{G}_e(\omega_n, \mathbf{k}) \Gamma_i \mathcal{G}_h(\omega_n, \mathbf{k}) \right] \\ &= -\sum_{\mathbf{k}, \eta = \pm} \left[F_i^\eta(\mathbf{k}) \frac{\tanh[\beta_c(E_\eta - \mu)/2]}{2(E_\eta - \mu)} \right], \end{aligned} \quad (4)$$

where ω_n are the fermionic Matsubara frequencies, $\beta_c = 1/(k_B T_c)$, and $\mathcal{G}_{e,h}$ are the normal Green's functions for electrons and holes, respectively. The matrices Γ_i are the vertex functions corresponding to the pairing channel whose forms are given in Table I. After performing the Matsubara summation, the susceptibility is expressed as a sum over the normal state energy bands, $E_\pm(\mathbf{k}) = \epsilon_0(\mathbf{k}) \pm \lambda_{\mathbf{k}}$, where $\lambda_{\mathbf{k}} = \sqrt{\varepsilon^2 + \alpha_{CR}^2 k^6}$. The coefficients F_{ij}^\pm depend on the projection of the pairing vertices onto the eigenvectors of the normal state Hamiltonian and are detailed in the Supplemental Material (SM) [45].

TABLE I. Classification of possible momentum-independent pairing potentials from the short-range interaction model. The pairings $\Delta_1, \Delta_2, \Delta_3$, and Δ_4 belong to the A_{1g}, A_{1u}, A_{2u} , and E_u irreps of D_{4h} , respectively. Matrix representations are given in the layer-spin basis, and transformation properties under inversion (\mathcal{I}) and mirror (\mathcal{M}_z) symmetries are listed.

Pairing	Operator representation	Matrix	\mathcal{I}	\mathcal{M}_z
Δ_1	$c_{l,\uparrow}c_{l,\downarrow} + c_{u,\uparrow}c_{u,\downarrow}, c_{l,\uparrow}c_{u,\downarrow} - c_{l,\downarrow}c_{u,\uparrow}$	$i\tau_0 s_y, i\tau_x s_y$	+	+
Δ_2	$i(c_{l,\uparrow}c_{u,\downarrow} + c_{l,\downarrow}c_{u,\uparrow})$	$\tau_y s_x$	-	-
Δ_3	$c_{l,\uparrow}c_{l,\downarrow} - c_{u,\uparrow}c_{u,\downarrow}$	$i\tau_z s_y$	-	-
Δ_4	$(i(c_{l,\uparrow}c_{u,\uparrow} + c_{l,\downarrow}c_{u,\downarrow}), c_{l,\uparrow}c_{u,\uparrow} - c_{l,\downarrow}c_{u,\downarrow})$	$(\tau_y s_z, i\tau_y s_0)$	-	+

The linearized gap equations for the different pairing channels are then constructed. For the even-parity A_{1g} channel (Δ_1), the intralayer (Δ_{1a}) and interlayer (Δ_{1b}) components belong to the same irrep and are thus coupled, leading to a matrix equation

$$\begin{vmatrix} U\chi_{1a,1a} - 1 & U\chi_{1a,1b} \\ V\chi_{1b,1a} & V\chi_{1b,1b} - 1 \end{vmatrix} = 0. \quad (5)$$

For the odd-parity channels Δ_2 (A_{1u}), Δ_3 (A_{2u}), and Δ_4 (E_u), which belong to distinct irreps, the gap equations are decoupled

$$V\chi_2 = 1, U\chi_3 = 1, V\chi_4 = 1. \quad (6)$$

By solving these equations, the superconducting phase diagram in the U - V plane is determined by identifying the pairing channel with the maximum critical temperature T_c . Figures 2(b)-2(d) show the resulting phase diagrams for three representative μ : μ_A , which intersects both the upper and lower bands, while μ_B and μ_C intersect only the lower band, with μ_B located within the HG [Fig. 2a]. The phase diagram reveals a rich landscape where three distinct superconducting states— Δ_1 , Δ_2 , and Δ_3 —compete for dominance against normal metallic phase. Δ_4 never emerges as the leading instability for the interactions considered. The outcome of this competition is dictated by the interplay between the intralayer (U) and interlayer (V) interactions. Specifically, a dominant attractive intralayer interaction ($U > 0$) stabilizes the conventional spin-singlet state Δ_1 . Conversely, when the interlayer interaction prevails ($|V| > U$), the system favors one of two unconventional spin-triplet phases, Δ_2 or Δ_3 . Δ_2 phase can be stabilized by a combination of repulsive intralayer and attractive interlayer interactions; however, this stabilization requires dominant V for μ_C . If both interactions are repulsive, no superconducting instability occurs, and the system remains in a normal metal.

The intralayer odd-parity Δ_3 is of primary focus of this work. Its stability region appears in cases μ_B and μ_C . The emergence of this odd-parity state as a ground state is plausible in realistic material settings, such as oxide interfaces, where superconductivity arises from a competition between screened Coulomb repulsion and phonon-mediated attraction. The parameters U and V represent the net effective interactions resulting from this interplay. It's reasonable to assume that both screening and phonon coupling are more effective within the

layers than between them. This asymmetry can create a scenario where the effective intralayer interaction U becomes attractive ($U > 0$) while the effective interlayer interaction V remains repulsive ($V < 0$). As seen in Figs. 2(c) and 2(d), the parameter regime with $U > 0$ and $V < 0$ strongly favors the Δ_3 pairing state, providing a well-motivated physical scenario for its realization.

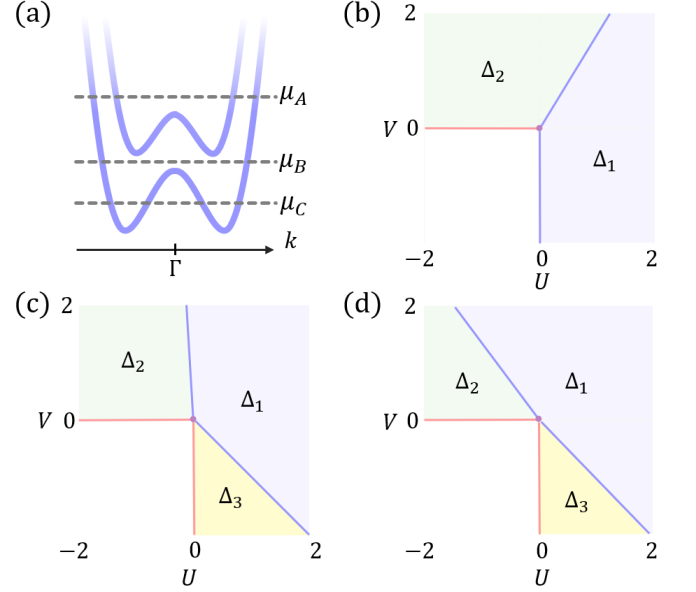


FIG. 2. (a) Energy dispersion at the Γ , illustrating the HG induced by ε . The chemical potential $\mu_A = 1.05$ intersects both upper and lower bands, while $\mu_B = -0.25$ and $\mu_C = -0.4$ intersect only the lower band. (b-d) Superconducting phase diagram for each chemical potential. The phases are color-coded as follows: Δ_1 (pale blue), Δ_2 (pale green), Δ_3 (pale yellow), and a non-superconducting phase (white). Common parameters, $\beta_0=0.5, \beta_1=-1, \varepsilon=0.35, \alpha_{CR}=0.1$.

Helical f -wave TSC.—We now analyze the topological properties of the superconducting phase driven by the order parameter Δ_3 . While the normal state respects the mirror symmetry \mathcal{M}_z , Δ_3 is odd under this operation, leading to a superconducting state that spontaneously breaks \mathcal{M}_z . The BdG Hamiltonian retains a modified mirror symmetry by introducing operator $\hat{\mathcal{M}}_z \equiv \text{diag}[\mathcal{M}_z, -\mathcal{M}_z^*]$ in the Nambu space. This extended symmetry allows the BdG Hamiltonian to be block-diagonalized into two sectors, corresponding to the mirror eigenvalues $\pm i$. The BdG Hamiltonian for each sector is

$\mathcal{H}_{\pm i}(\mathbf{k})$, where

$$\mathcal{H}_{\pm i}(\mathbf{k}) = \begin{pmatrix} \mathcal{H}_{N,\pm i}(\mathbf{k}) + \mu & -i\Delta_0 s_y \\ i\Delta_0 s_y & -\mathcal{H}_{N,\pm i}^*(-\mathbf{k}) - \mu \end{pmatrix},$$

with $\mathcal{H}_{N,\pm i}(\mathbf{k}) = -\epsilon_0(\mathbf{k})s_0 - \mathbf{g}_{\text{CR}}(\mathbf{k}) \cdot \mathbf{s} \pm \epsilon s_z$, and μ_B located within the HG. $\mathcal{H}_{+i}(\mathbf{k})$ and $\mathcal{H}_{-i}(\mathbf{k})$ lack TRS individually, but are mapped onto each other by TRS operator \mathcal{T} . To reveal the effective pairing symmetry induced by Δ_3 , we project the Hamiltonian $\mathcal{H}_{\pm i}$ onto the basis of the normal-state spin-split bands, $\mathcal{H}_{N,\pm i}$. Focusing on the $+i$ block, we project the Δ_3 pairing potential (which is proportional to $-is_y$ in this subspace) onto the upper (+) and lower (-) bands. The projected potentials are [45]

$$\begin{aligned} \Delta_{++}(\mathbf{k}) &= -\Delta_0 \frac{\alpha_{\text{CR}}}{\lambda_{\mathbf{k}}} \left(-ik_x + k_y \right)^3, \\ \Delta_{+-}(\mathbf{k}) &= -\Delta_0 \frac{\epsilon}{\lambda_{\mathbf{k}}}, \\ \Delta_{--}(\mathbf{k}) &= -\Delta_0 \frac{\alpha_{\text{CR}}}{\lambda_{\mathbf{k}}} \left(ik_x + k_y \right)^3. \end{aligned} \quad (7)$$

This result is central to our work: the triple-winding spin texture of the normal state, encoded in the cubic momentum dependence of $\mathbf{g}_{\text{CR}}(\mathbf{k})$, is directly inherited by the intraband pairing potential. The resulting gap functions, $\Delta_{++}(\mathbf{k}) \propto (k_y - ik_x)^3$ and $\Delta_{--}(\mathbf{k}) \propto (k_y + ik_x)^3$ correspond to $f_{y(3x^2-y^2)} \mp if_{x(x^2-3y^2)}$ symmetries with opposite chiralities for the upper and lower bands. When μ lies within the HG [Fig. 2(a)], only the lower band crosses μ . The system is then effectively a single band superconductor. In this regime, the \mathcal{H}_{+i} sector describes a chiral f -wave TSC. The \mathcal{H}_{-i} sector describes the time-reversed partner with opposite chirality. Together, they form a TRS-invariant TSC with helical f -wave pairing protected by mirror symmetry \mathcal{M}_z .

Since each mirror subsector belongs to class D, its topology is characterized by an integer Chern number, $\mathcal{N}_{\pm i}$. The overall topology of the system is classified by the MCN $\mathcal{N}_M = (\mathcal{N}_{+i} - \mathcal{N}_{-i})/2$ [46–52]. A direct calculation shows that when μ is inside the HG and the system is fully gapped (requiring $\epsilon^2 > \mu^2 + \Delta_0^2$), the MCN is $\mathcal{N}_M = 3$. The magnitude \mathcal{N}_M directly reflects the triple-winding topology of the cubic Rashba spin texture [Fig. 1(a)], which has been faithfully transferred to the superconducting order parameter. This demonstrates the “topology multiplier” principle: the threefold winding of the spin texture generates a threefold enhancement of the topological invariant. The bulk-boundary correspondence dictates that a TSC with MCN \mathcal{N}_M will host $|\mathcal{N}_M|$ pairs of counterpropagating Majorana edge modes. To verify this, we discretize the model on a square lattice and calculate the spectral function $\mathcal{A}(E, \mathbf{k})$ for a semi-infinite geometry. As shown in Fig. 3(a), $\mathcal{A}(E, \mathbf{k})$ for the Δ_3 phase with $\mathcal{N}_M = 3$ clearly shows three pairs of linearly dispersing, gapless modes crossing zero energy. These are the predicted three helical Majorana channels, in stark contrast to the single pair expected from conventional linear RSOC [22–24].

For μ_C , which features two concentric FSs enclosing the Γ point, Δ_3 remains favored when $U > 0$ and $V < 0$. Apply-

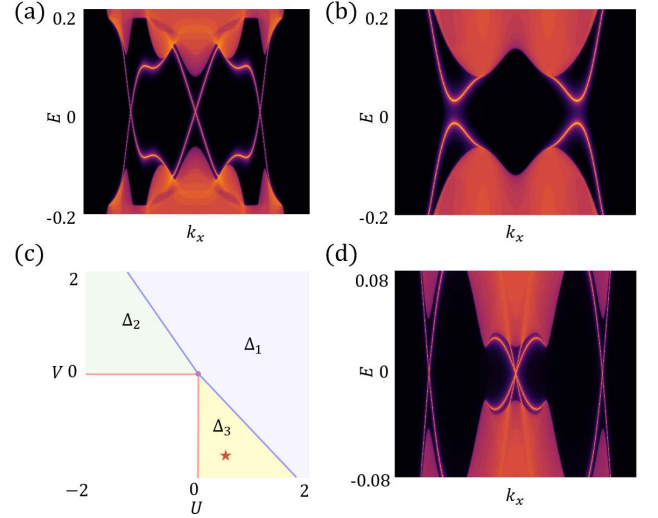


FIG. 3. Superconducting phase diagram and spectral function $\mathcal{A}(E, \mathbf{k})$ for the Δ_3 pairing phase in a semi-infinite geometry. (a), (b) $\mathcal{A}(E, k_x)$ for the pure cubic RSOC case ($\alpha_{\text{CR}} = 0.1$). Three Kramers pairs of Majorana edge modes appear when the chemical potential is in HG as in (a) $\mu_B = -0.2$, but not outside it as in (b) $\mu_C = -0.6$. (c) Phase diagram of coexisting linear and cubic RSOCs $\alpha_{\text{CR}} = \alpha_{\text{LR}} = 0.1$ at $\mu_C = -0.4$. (d) $\mathcal{A}(E, k_x)$ at the point marked by red star in (c), revealing four pairs of helical Majorana modes. Common parameters: $\beta_0 = 0.5, \beta_1 = -1, \epsilon = 0.35, \Delta_0 = 0.2$.

ing the established topological criterion for odd-parity superconductors [19, 20], this superconducting state is found to be topologically trivial [Fig. 3(b)]. This is a direct consequence of the even number of FSs enclosing the TRS invariant momentum. This scenario is also observed in pure linear RSOC bilayer [23]. However, this classification is fundamentally altered when cubic and linear RSOCs coexist.

Helical hybrid $p + f$ -wave TSC.—A critical test for experimental relevance is the stability of a topological phase against perturbations expected in real materials. For instance, in oxide heterostructures like LAO/STO [31, 38], both linear and cubic RSOCs coexist, with their relative strengths tunable via carrier filling. We therefore investigated the robustness of the $\mathcal{N}_M = 3$ phase by reintroducing the linear RSOC. We found that the three pairs of helical Majorana edge modes persist for dominant cubic RSOC as long as μ lies within HG (See SM[45]).

Crucially, a new phenomenon emerges when μ is moved out of HG but remains within the lower band. This creates two distinct FSs: a smaller, inner surface near the Γ point and a larger, outer surface farther away [Fig. 1(b)]. In this regime Δ_3 pairing remains favored under similar interaction conditions [Fig. 3(c)]. The interplay between coexisting linear and cubic RSOCs and Δ_3 pairing induces an even richer TSC characterized by a heightened MCN, $\mathcal{N}_M = 4$, hosting four Kramers pairs of Majorana edge modes [Fig. 3(d)]. This state is a beautiful example of \mathbf{k} -space topological engineering. The different momentum scaling of the two RSOCs allows them to dominate in different regions of the Brillouin zone. Given sufficient

separation of the FSs in k -space, the linear term ($\propto k$) dominates the inner surface, fostering a helical p -wave state. Conversely, the cubic term ($\propto k^3$) dominates the outer surface, fostering a helical f -wave state. The resulting superconductor effectively merges these two distinct topologies, summing their respective contributions to the total MCN.

Discussion and conclusion.—We introduce a novel mechanism for a helical f -wave topological crystalline superconductor, driven by the interplay between odd-parity pairing and cubic RSOC in locally noncentrosymmetric systems. The unique triple-winding spin texture inherent to cubic RSOC yields a TSC with a high MCN $\mathcal{N}_M=3$, protecting three pairs of helical Majorana edge modes. Furthermore, we reveal a remarkable duality: the interplay of linear and cubic RSOCs allows both helical p -wave and f -wave pairing to emerge simultaneously on two distinct FSs enclosing the Γ point. Our bilayer RSOC model is applicable to tunable, locally noncentrosymmetric materials, such as LAO/STO superlattices and strained germanium quantum wells. Notably, bilayer 2D electron gas has been realized in LAO/STO [53]. The exceptional tunability of these platforms facilitates a full exploration of the phase diagram, potentially achieving TSCs with $\mathcal{N}_M=3, 4$. Alternatively, an effective odd-parity state can be engineered by proximitizing cubic Rashba layers with s -wave superconductors arranged with a π -phase difference, analogous to those proposed in other locally noncentrosymmetric multilayers [54, 55].

While we have primarily focused on Δ_3 , the model also supports interlayer pairing Δ_2 , which can give rise to a helical f -wave TSC. Moreover, the model admits a pairing in the 2D E_u irrep (Δ_4 in Table I), leading to a nematic superconductor that spontaneously breaks the crystal's rotational symmetry in the superconducting gap [45]. Although not the leading instability, the emergence of this nematic phase underscores a significant consequence of cubic RSOC.

Acknowledgments.—We thank Da-Shuai Ma, Zhongbo Yan, and Noah F.Q. Yuan for helpful discussions. This work was supported by the National Natural Science Foundation of China (NSFC, Grants No. 12474151, No. 12222402, and 12347101), and Beijing National Laboratory for Condensed Matter Physics (No. 2024BNLCMPKF025).

* These authors contributed equally to this work.

† hu.lunhui.zju@gmail.com

‡ rcwang@cqu.edu.cn

§ donghuixu@cqu.edu.cn

- [1] Y. A. Bychkov and É. I. Rashba, Properties of a 2d electron gas with lifted spectral degeneracy, *JETP lett* **39**, 78 (1984).
- [2] A. Manchon, H. C. Koo, J. Nitta, S. M. Frolov, and R. A. Duine, New perspectives for Rashba spin-orbit coupling, *Nature Mater.* **14**, 871 (2015).
- [3] G. Bihlmayer, P. Noël, D. V. Vyalikh, E. V. Chulkov, and A. Manchon, Rashba-like physics in condensed matter, *Nat. Rev. Phys.* **4**, 642 (2022).
- [4] J. Sinova, D. Culcer, Q. Niu, N. A. Sinitsyn, T. Jungwirth, and A. H. MacDonald, Universal intrinsic spin Hall effect, *Phys. Rev. Lett.* **92**, 126603 (2004).
- [5] M. Z. Hasan and C. L. Kane, Colloquium: Topological insulators, *Rev. Mod. Phys.* **82**, 3045 (2010).
- [6] X.-L. Qi and S.-C. Zhang, Topological insulators and superconductors, *Rev. Mod. Phys.* **83**, 1057 (2011).
- [7] L. P. Gor'kov and E. I. Rashba, Superconducting 2D system with lifted spin degeneracy: Mixed singlet-triplet state, *Phys. Rev. Lett.* **87**, 037004 (2001).
- [8] S. K. Yip, Two-dimensional superconductivity with strong spin-orbit interaction, *Phys. Rev. B* **65**, 144508 (2002).
- [9] P. A. Frigeri, D. F. Agterberg, A. Koga, and M. Sigrist, Superconductivity without inversion symmetry: MnSi versus CePt₃Si, *Phys. Rev. Lett.* **92**, 097001 (2004).
- [10] X. Zhang, Q. Liu, J.-W. Luo, A. J. Freeman, and A. Zunger, Hidden spin polarization in inversion-symmetric bulk crystals, *Nat. Phys.* **10**, 387 (2014).
- [11] K. Gotlieb, C.-Y. Lin, M. Serbyn, W. Zhang, C. L. Smallwood, C. Jozwiak, H. Eisaki, Z. Hussain, A. Vishwanath, and A. Lanzara, Revealing hidden spin-momentum locking in a high-temperature cuprate superconductor, *Science* **362**, 1271 (2018).
- [12] S. Khim, J. Landaeta, J. Banda, N. Bannor, M. Brando, P. Brydon, D. Hafner, R. K uchler, R. Cardoso-Gil, U. Stockert, et al., Field-induced transition within the superconducting state of CeRh₂As₂, *Science* **373**, 1012 (2021).
- [13] M. H. Fischer, M. Sigrist, D. F. Agterberg, and Y. Yanase, Superconductivity and local inversion-symmetry breaking, *Annu. Rev. Condens. Matter Phys.* **14**, 153 (2023).
- [14] L. Fu and C. L. Kane, Superconducting proximity effect and majorana fermions at the surface of a topological insulator, *Phys. Rev. Lett.* **100**, 096407 (2008).
- [15] S. Fujimoto, Topological order and non-abelian statistics in noncentrosymmetric s -wave superconductors, *Phys. Rev. B* **77**, 220501 (2008).
- [16] M. Sato, Y. Takahashi, and S. Fujimoto, Non-Abelian topological order in s -wave superfluids of ultracold Fermionic atoms, *Phys. Rev. Lett.* **103**, 020401 (2009).
- [17] J. D. Sau, R. M. Lutchyn, S. Tewari, and S. Das Sarma, Generic new platform for topological quantum computation using semiconductor heterostructures, *Phys. Rev. Lett.* **104**, 040502 (2010).
- [18] J. Alicea, Majorana fermions in a tunable semiconductor device, *Phys. Rev. B* **81**, 125318 (2010).
- [19] L. Fu and E. Berg, Odd-parity topological superconductors: Theory and application to Cu_xBi₂Se₃, *Phys. Rev. Lett.* **105**, 097001 (2010).
- [20] M. Sato, Topological odd-parity superconductors, *Phys. Rev. B* **81**, 220504 (2010).
- [21] X.-L. Qi, T. L. Hughes, and S.-C. Zhang, Topological invariants for the fermi surface of a time-reversal-invariant superconductor, *Phys. Rev. B* **81**, 134508 (2010).
- [22] C.-X. Liu and B. Trauzettel, Helical Dirac-Majorana interferometer in a superconductor/topological insulator sandwich structure, *Phys. Rev. B* **83**, 220510 (2011).
- [23] S. Nakosai, Y. Tanaka, and N. Nagaosa, Topological superconductivity in bilayer Rashba system, *Phys. Rev. Lett.* **108**, 147003 (2012).
- [24] F. Zhang, C. L. Kane, and E. J. Mele, Time-reversal-invariant topological superconductivity and Majorana Kramers pairs, *Phys. Rev. Lett.* **111**, 056402 (2013).
- [25] F. Zhang, C. L. Kane, and E. J. Mele, Topological mirror superconductivity, *Phys. Rev. Lett.* **111**, 056403 (2013).
- [26] H. Nakamura, T. Koga, and T. Kimura, Experimental evidence of cubic Rashba effect in an inversion-symmetric oxide, *Phys. Rev. Lett.* **108**, 206601 (2012).

- [27] Z. Zhong, A. Tóth, and K. Held, Theory of spin-orbit coupling at $\text{LaAlO}_3/\text{SrTiO}_3$ interfaces and SrTiO_3 surfaces, *Phys. Rev. B* **87**, 161102 (2013).
- [28] R. Moriya, K. Sawano, Y. Hoshi, S. Masubuchi, Y. Shiraki, A. Wild, C. Neumann, G. Abstreiter, D. Bougeard, T. Koga, and T. Machida, Cubic Rashba spin-orbit interaction of a two-dimensional hole gas in a strained-Ge/SiGe quantum well, *Phys. Rev. Lett.* **113**, 086601 (2014).
- [29] Y. Kim, R. M. Lutchyn, and C. Nayak, Origin and transport signatures of spin-orbit interactions in one- and two-dimensional SrTiO_3 -based heterostructures, *Phys. Rev. B* **87**, 245121 (2013).
- [30] P. Kim, K. T. Kang, G. Go, and J. H. Han, Nature of orbital and spin Rashba coupling in the surface bands of SrTiO_3 and KTaO_3 , *Phys. Rev. B* **90**, 205423 (2014).
- [31] W. Lin, L. Li, F. Doğan, C. Li, H. Rotella, X. Yu, B. Zhang, Y. Li, W. S. Lew, S. Wang, *et al.*, Interface-based tuning of Rashba spin-orbit interaction in asymmetric oxide heterostructures with 3 d electrons, *Nat. Commun.* **10**, 3052 (2019).
- [32] D. Y. Usachov, I. A. Nechaev, G. Poelchen, M. Güttler, E. E. Krasovskii, S. Schulz, A. Generalov, K. Kliemt, A. Kraiker, C. Krellner, K. Kummer, S. Danzenbächer, C. Laubschat, A. P. Weber, J. Sánchez-Barriga, E. V. Chulkov, A. F. Santander-Syro, T. Imai, K. Miyamoto, T. Okuda, and D. V. Vyalikh, Cubic Rashba effect in the surface spin structure of rare-earth ternary materials, *Phys. Rev. Lett.* **124**, 237202 (2020).
- [33] H. J. Zhao, H. Nakamura, R. Arras, C. Paillard, P. Chen, J. Gosteau, X. Li, Y. Yang, and L. Bellaiche, Purely cubic spin splittings with persistent spin textures, *Phys. Rev. Lett.* **125**, 216405 (2020).
- [34] J. Schliemann and D. Loss, Spin-hall transport of heavy holes in III – V semiconductor quantum wells, *Phys. Rev. B* **71**, 085308 (2005).
- [35] O. Bleibaum and S. Wachsmuth, Spin hall effect in semiconductor heterostructures with cubic rashba spin-orbit interaction, *Phys. Rev. B* **74**, 195330 (2006).
- [36] J. Zhou, W.-Y. Shan, and D. Xiao, Spin responses and effective hamiltonian for the two-dimensional electron gas at the oxide interface $\text{LaAlO}_3/\text{SrTiO}_3$, *Phys. Rev. B* **91**, 241302 (2015).
- [37] X.-T. Peng, F. Lin, L. Chen, L. Li, D.-H. Xu, and J.-H. Sun, Tunable correlation effects of magnetic impurities by cubic Rashba spin-orbit coupling, *Phys. Rev. B* **107**, 165148 (2023).
- [38] A. D. Caviglia, M. Gabay, S. Gariglio, N. Reyren, C. Cancellieri, and J.-M. Triscone, Tunable Rashba spin-orbit interaction at oxide interfaces, *Phys. Rev. Lett.* **104**, 126803 (2010).
- [39] N. Reyren, S. Thiel, A. Caviglia, L. F. Kourkoutis, G. Hammerl, C. Richter, C. W. Schneider, T. Kopp, A.-S. Ruetschi, D. Jaccard, *et al.*, Superconducting interfaces between insulating oxides, *Science* **317**, 1196 (2007).
- [40] A. Caviglia, S. Gariglio, N. Reyren, D. Jaccard, T. Schneider, M. Gabay, S. Thiel, G. Hammerl, J. Mannhart, and J.-M. Triscone, Electric field control of the $\text{LaAlO}_3/\text{SrTiO}_3$ interface ground state, *Nature* **456**, 624 (2008).
- [41] L. Mao, J. Shi, Q. Niu, and C. Zhang, Superconducting phase with a chiral f -wave pairing symmetry and Majorana Fermions induced in a hole-doped semiconductor, *Phys. Rev. Lett.* **106**, 157003 (2011).
- [42] M. Alidoust, C. Shen, and I. Žutić, Cubic spin-orbit coupling and anomalous Josephson effect in planar junctions, *Phys. Rev. B* **103**, L060503 (2021).
- [43] M. Luethi, K. Laubscher, S. Bosco, D. Loss, and J. Klinovaja, Planar Josephson junctions in germanium: Effect of cubic spin-orbit interaction, *Phys. Rev. B* **107**, 035435 (2023).
- [44] T. Hashimoto, S. Kobayashi, Y. Tanaka, and M. Sato, Superconductivity in doped Dirac semimetals, *Phys. Rev. B* **94**, 014510 (2016).
- [45] See Supplemental Material for (Sec. SI) bilayer Rashba spin-orbit coupled model and symmetries, (Sec. SII) interacting Hamiltonian and symmetry classification of pairing channels, (Sec. SIII) linearized gap equation and superconducting phase diagrams, (Sec. SIV) topological superconductors induced by odd-parity pairing and Rashba spin-orbit couplings, (Sec. SV) nematic superconductivity induced by the E_u irrep.
- [46] J. C. Y. Teo, L. Fu, and C. L. Kane, Surface states and topological invariants in three-dimensional topological insulators: Application to $\text{Bi}_{1-x}\text{Sb}_x$, *Phys. Rev. B* **78**, 045426 (2008).
- [47] Y. Ueno, A. Yamakage, Y. Tanaka, and M. Sato, Symmetry-protected Majorana Fermions in topological crystalline superconductors: Theory and application to Sr_2RuO_4 , *Phys. Rev. Lett.* **111**, 087002 (2013).
- [48] C.-K. Chiu, H. Yao, and S. Ryu, Classification of topological insulators and superconductors in the presence of reflection symmetry, *Phys. Rev. B* **88**, 075142 (2013).
- [49] Y. Tsutsumi, M. Ishikawa, T. Kawakami, T. Mizushima, M. Sato, M. Ichioka, and K. Machida, UPt_3 as a topological crystalline superconductor, *J. Phys. Soc. Jpn.* **82**, 113707 (2013).
- [50] K. Shiozaki and M. Sato, Topology of crystalline insulators and superconductors, *Phys. Rev. B* **90**, 165114 (2014).
- [51] Y. Ando and L. Fu, Topological crystalline insulators and topological superconductors: From concepts to materials, *Annu. Rev. Condens. Matter Phys.* **6**, 361 (2015).
- [52] T. Yoshida, M. Sigrist, and Y. Yanase, Topological crystalline superconductivity in locally noncentrosymmetric multilayer superconductors, *Phys. Rev. Lett.* **115**, 027001 (2015).
- [53] H. J. H. Ma, Z. Huang, W. M. Lü, A. Annadi, S. W. Zeng, L. M. Wong, S. J. Wang, T. Venkatesan, and Ariando, Tunable bilayer two-dimensional electron gas in $\text{LaAlO}_3/\text{SrTiO}_3$ superlattices, *Appl. Phys. Lett.* **105**, 011603 (2014).
- [54] T. Yoshida, M. Sigrist, and Y. Yanase, Topological crystalline superconductivity in locally noncentrosymmetric multilayer superconductors, *Phys. Rev. Lett.* **115**, 027001 (2015).
- [55] Y. Volpez, D. Loss, and J. Klinovaja, Second-order topological superconductivity in π -junction rashba layers, *Phys. Rev. Lett.* **122**, 126402 (2019).